Smartfloat: A Multimodal Underwater Vehicle Combining Float and Glider Capabilities

JUNJUN CAO, (Student Member, IEEE), **DI LU, DAIWEI LI**, (Student Member, IEEE), **ZHENG ZENG, BAOHENG YAO, AND LIAN LIAN**
State Key Laboratory of Ocean Engineering, Shanghai Jiao Tong University (SJTU), Shanghai 200240, China
Corresponding author: Lian Lian (llian@sjtu.edu.cn)

ABSTRACT This paper proposes a novel hybrid underwater vehicle, the *Smartfloat*, which integrates the concept of buoyancy-driven underwater gliders and conventional profiling floats. The vehicle is presented to address the challenges in ocean monitoring, such as the multidisciplinary observations of long-range transport of the mesoscale features with high spatial-temporal resolution. The vehicle combines the mechanisms of Argo profiling float and the underwater glider, with the application of a special designed attitude control system and the ingenious general arrangement. The vehicle can switch the operating mode between drifting mode and gliding mode. Such a multimodal vehicle would merge the benefits of making measurements in a very energy-efficient way when drifting with the currents in Argo mode, and operating as an underwater glider in glider mode when it is needed to cross the ocean eddies, ocean fronts, filaments, or some stirring regions. In this paper, a proof-of-concept platform including its concept of operations, the main components and subsystems design, and the correlative mathematical analysis is introduced in detail. Experiments in field trials are presented to characterize and illustrate each mode of operation and repeated mode transitions. The results demonstrate the feasibility and the good performance of the proposed vehicle.

INDEX TERMS Autonomous vehicle, ocean monitoring, profiling float, multimodal underwater vehicle, underwater glider.

I. INTRODUCTION

The ocean change is one of the most important consequences of ongoing global climate system because they transport heat and fresh water, and exchange these with the atmosphere. For the period 2003-2014, the rate of observed sea level has been rising at a rate between 2.8 and 3.6 mm per year with significant low-frequency variability superimposed [1]. Sea level variation is spatially non-uniform. Over this time span, the steric sea level contribution, essentially estimated from Argo-based ocean temperature and salinity data, varies from -0.5 ± 0.5 mm/year to $+0.8\pm0.8$ mm/year [2]. In all these global climate observations, the Argo-base ocean observing method plays a significant role in understanding and analyzing the ocean change [3],[4].

As we know, the profiling floats reciprocate between the surface and the predetermined depth of the ocean to measure the ocean and upload environment data such as ocean current, thermocline and halocline [5]–[7]. As for the current profiling

floats, they have been experimentally verified with the ability of sustaining effort for two or even three years, which is assessed by the operating method [8]. Nevertheless, the Argo profiling float can only drift with the ocean currents but not able to achieve reliable trajectories tracking. This makes the position of the Argo-based measurements uncontrollable and difficult to predict. In some specific situations, the scientists are more concerned about the internal status and mechanism of ocean phenomena like eddy current [9], and a resulting internal tracking measurement of these phenomena are expected. However, the Argo profiling floats are apparently incompetent in these mission scenarios.

Besides the Lagrange profiling float, underwater gliders (UGs), a kind of autonomous underwater vehicles with maneuverability, have also shown powerful performance in sampling and exploring the ocean environment [10]–[12], especially in high spatial-temporal and multidisciplinary oceanic observations [13]. UG is an indispensable underwater detection apparatus. Compared with the profiling float, the outstanding advantage of UG is the capability of active traversing hundreds of kilometers for weeks or even months.

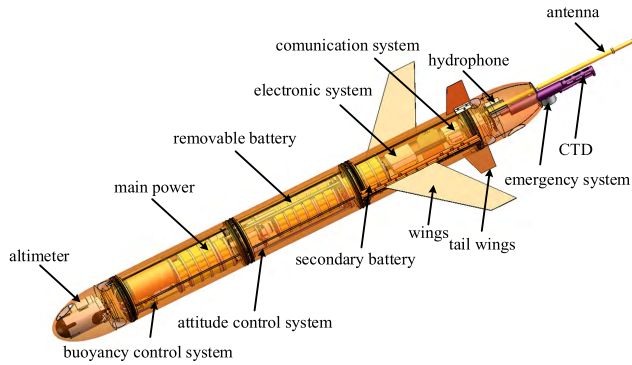The associate editor coordinating the review of this manuscript and approving it for publication was Zeyang Xia.

FIGURE 2. The operation strategies of profiling float and underwater glider.

FIGURE 3. Operation strategies of the multimodal underwater vehicle.

UG is commonly shaped like a fixed-wing airplane. It can obtain maneuverability and often equips with various sensors to consummate the oceanic data collection. While travelling through the water column, the glider performs a vertical zigzag movement to go forward by adjusting the buoyancy and the positional relationship between the center of gravity and buoyancy. The forward driving force that results in a forward horizontal displacement is the horizontal component of the lift force generated by the fixed wings [14], [15].

The gliders have been successfully tested to overcome comparatively current and collect specific marine information around the stirring regions. Recently, a number of novel underwater gliders have been developed to obtain better performance on measuring methods except the conventional profiling floats and the legacy gliders [16]–[18]. These technologies improve the gliders by minimizing transit time [19], enhancing robustness in currents [20], or increasing the maneuverability in coastal regions [21]. Despite that UGs are robust ocean sampling platforms that are increasingly being deployed in some complex current regions [22]–[24], their endurance, which is often limited to about 3 to 6 months depending on battery design capacity, is much inferior to profiling drifting float [25].

A desired ocean observing platform would have the combined positive attributes of an underwater glider and the long endurance as Argo profiling float [26], [27]. This paper proposes a novel hybrid multimodal underwater vehicle, the *Smartfloat*, shown in Fig. 1 [28]. The *Smartfloat* integrates the concept of buoyancy-driven underwater gliders and conventional profiling floats. The superiority of the combination is the achievement of extending endurance greatly for current UG technology and acquiring controllability for current Argo profiling float in one single platform. The *Smartfloat* is designed to achieve more than 110 profiles with 4000 meters operating depth in float mode while it can glide underwater with a continuously working range of thousand kilometers, carrying with CTD, chlorophyll, CDOM, hydrophone and other measuring equipment in glider mode. The measurement data is reported in real time via satellite communications once it surfaces. As a remarkable feature, the design endurance of the *Smartfloat* is more than 3 years.
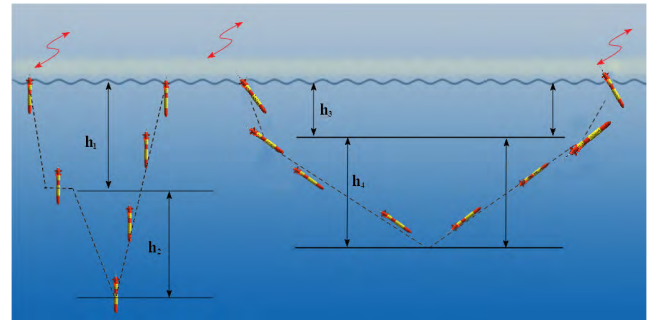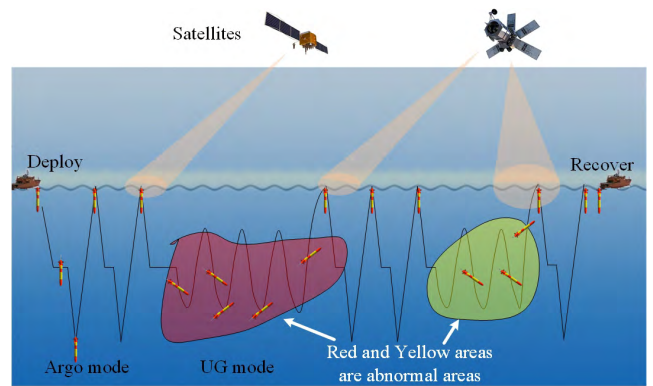
It is known that the float is designed to observe the ocean by drifting with the flow. Since there is no need to change the attitude, the platform's center of gravity (CG) is designed to always stay under the center of buoyancy (CB), which can make the float consistent vertical and stable in water. On the contrary, a UG needs to change its attitude to a non-vertical state to perform a forward glide during the operation. However, to ensure the vehicle is bottom heavy for stable gliding underwater, the CG and the CB of a UG are designed to be never able to align to the central longitudinal axis.

Therefore, realizing the combination of the UG and the profiling float is mainly to break the limitation of the attitude adjustment of each platform and enable a full range of pitch variation in for the *Smartfloat*. This paper presents a novel design approach that allows a necessary change of the CG for the requirements of both underwater glide and vertical float. By using the special designed attitude control system and the ingenious general arrangement, the multimodal underwater vehicle can switch between Argo mode and UG mode. When using the attitude control system to obtain a steady vertical state, the proposed vehicle can drift with the currents for about 10 days and make measurements with minimum energy consumption by only controlling its buoyancy. When using the attitude control system to obtain a variable non-vertical attitude, the proposed vehicle can realize locomotion underwater through gliding by a joint control of its buoyancy and the position of CG. The operation scheme of the proposed multimodal vehicle is shown in Fig. 3.
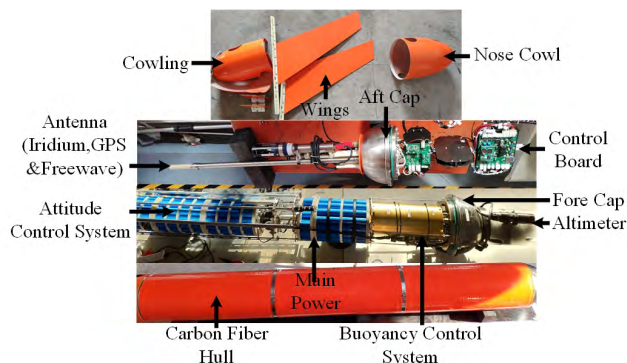
FIGURE 4. *Smartfloat* vehicle.

The remainder of the paper is organized as follows. The mechanical design and mass configuration of the vehicle is introduced in Section II. The next section presents the attitude control strategy for the vehicle. Then, Section IV presents the simulation and experiment results. Finally, Section V draws the conclusion of the work.

II. CONFIGURATION AND MECHANICS DESIGN

The newly multimodal underwater vehicle named *Smartfloat* can switch between the normal glider mode and the normal float mode, which is achieved by the special mechanics and configuration design of the vehicle.

A. MECHANICAL DESIGN

The vehicle has a streamline profile with simple hydrodynamic characteristics. The main body functioned as pressure hull consists of a 0.301 m diameter acrylic tube with a length of 2.5 m and two hemispherical end-caps. The caps are round to gain a high strength-to-weight ratio and contribute to streamline configuration, improving the aesthetics, and minimizing the drag of the hull as well [28]. UGs and profiling floats reach various depth by controlling either the weight or the buoyancy (volume). The *Smartfloat* shown in Fig. 4 adjusts its attitude in the same way as conventional UGs by changing its buoyancy and the position of the internal mass. In the designs of the glider and the float, most of the vehicle's mass should be distributed uniformly around the hull's axial column except a portion of the mass should be located at bottom, which is called ''bottom-heaviness'' [29]. The *Smartfloat* has an internal movable mass located in the middle of the body and a highly integrated buoyancy system mounted in the front cap.

The buoyancy control system is a crucially important part for underwater vehicle [30]. The schematic diagram and the configuration of the devised buoyancy system shown in Fig. 5 and Fig. 6, respectively. The vehicle regulates its displacement by pumping oil in or out the external oil sac. To increase buoyancy, a hydro Leduc PB33 HP micro-pump pumps the oil from the internal oil tank through the flowmeter and the one-way check valve into a 4L cylinder oil sac. To reduce buoyancy, the hydraulic oil passively flows through the motor operated valve and the zero leakage reversing
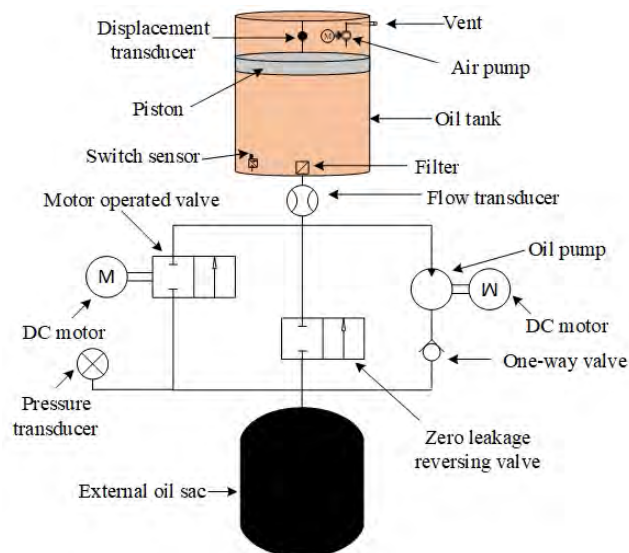

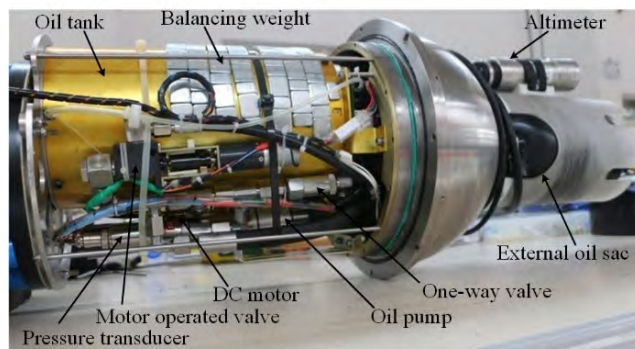**FIGURE 5.** Schematic diagram of buoyancy control system.

FIGURE 6. The buoyancy control system (For space-efficient assembling, the air pump and displacement transducer are mounted inside the oil tank, include the filter and switch sensor.).
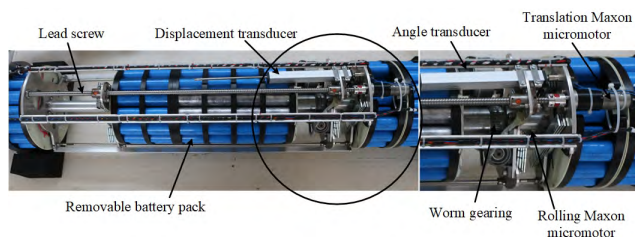

FIGURE 7. The attitude control system.

valve back to the inner tank from the sac under the ambient pressure. Making use of the ambient pressure for oil return-, is of benefit to energy saving and enables the proper function of the buoyancy system.

It is known that the UG and the profiling float have different requirements of the locations of the CG and the CB. To combine the motion patterns of UG and profiling float, an attitude control system of the vehicle exhibited in Fig. 7 is specially designed. The pitch, roll and yaw angles of the vehicle are controlled by the proper translation and rotation of the movable mass that is composed of lithium battery packs. For feedback control, a potentiometer and a compass are used

to measure the position and the angle of the battery packs. The pack is driven by a ball-screw-motor system to translate along the central axis within a range of ±8 cm and can be rotated 360° around the axis by a turbo-worm system, which ultimately results in a pitch regulation of ±60° and a roll regulation of ±40° when the vehicle is in UG mode. Due to the capability of full rotation of the movable pack, the vehicle can change to a vertical nose-down attitude, i.e., 90° pitch angle, to enter the profiling float mode by rotating the pack with 180°. Therefore, the main devised concept of operation modes switch is realized.

B. CONFIGURATION

The *Smartfloat* has its buoyancy engine located in the nose of the vehicle and has the movable mass moving within a limited range inside the body. In this paper, the vehicle's mass is divided into three parts in a similar way as the conventional design of a UG. The classification helps to simplify the task trying to study what an impact an action of movable mass can make on vehicle's attitude. The first part is referred to the stationary mass, m_{rs}, with its weight denoted as W_{rs} to represent all the components whose mass and the position of its gravity center will not change during the operation. For the purpose of realizing the combination of the UG mode and the profiling float mode via the movable mass, the stationary mass is designed in a place with an offset, z_{wrs}, in the positive z-axis direction from the central body x-axis in which the CB is. The second part is only the movable mass, m_{mr}. Its weight is denoted as W_{mr} and acts at a distance z_{mr} below the body x-axis. Due to the special mechanical design, the roll control of the movable mass can reach a full 360° which differs from the traditional UG with limited roll range. The third part is the oil mass, m_o, with a denotation W_o for its weight. This mass is used to adjust the buoyancy of the vehicle via changing the displaced volume of the external oil bladder. Note that the oil mass is distributed partially in the tank (m_{o1} or W_{o1}) while the rest is in the bladder (m_{o2} or W_{o1}). As for the vehicle's buoyancy, it is considered as the total of the buoyancy of the main body that denoted as B_{rs} and the buoyancy of the external oil sac that denoted as Bb. A static force analysis with respect to the vehicle loitering in steady water with zero-velocity and a fixed pitch angle (θ) are shown in Fig. 8. From the figure, it can be inferred that the regulations of the external oil bladder and the movable mass all contribute to the pitch adjustment, and the rotation of the movable mass is the actuation of the rolling motion of the vehicle as well.

As shown in the Fig. 8, the longitudinal location of these forces are measured from the nose cap of the vehicle. Given the static equilibrium state of the vehicle, the following relationships are always held:

$$\sum F_z : W_{mr} + W_{o1} + W_{o2} + W_{rs} - B_b - B_{rs} = 0 \quad (1)$$

$$\sum M : (x_{mr} + z_{mr} \tan\theta)W_{mr} + x_{o1}W_{o1} + x_{o2}W_{o2} + (x_{wrs} + z_{wrs} \tan\theta)W_{rs} - x_bB_b - x_{brs}B_{rs} = 0 \quad (2)$$

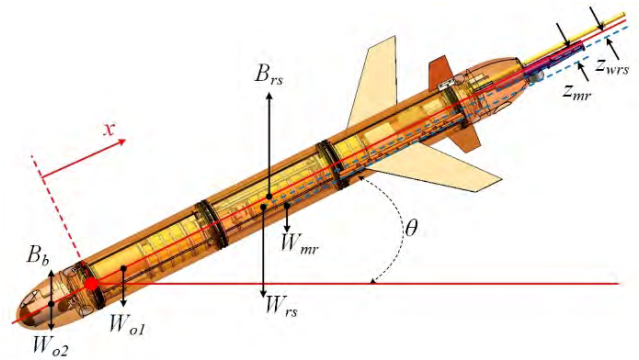**FIGURE 8.** The 3D illustration and mass definitions of the vehicle. Forces acting on vehicle loitering in steady water with a zero-velocity and a pitch angle. The longitudinal positions where the forces act are measured from the original of body frame and indicated by x (x_{mr}, x_{o1}, x_{o2}, x_{wrs}, x_b, x_{brs}).
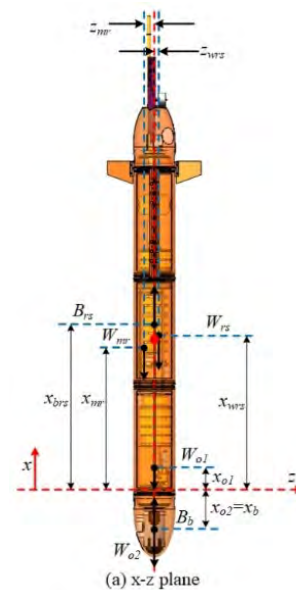
FIGURE 9. The 3D illustration and mass definitions of the vehicle. Forces acting on vehicle loitering in steady water with a zero-velocity and a pitch angle. The longitudinal positions where the forces act are measured from the original of body frame and indicated by x (x_{mr}, x_{o1}, x_{o2}, x_{wrs}, x_b, x_{brs}).

Same as the conventional UG design, the bottom-heaviness is critical to the vehicle's stability in both pitch and roll maneuvers. However, the proposed vehicle will experience a significant variation of the bottom-heaviness in the modes transition process. When the vehicle is in profiling float mode, the designed bottom-heaviness is very low to guarantee a stable float in vertical nose-down attitude. When in the glider mode, the CG of the vehicle needs to shift to the front or the back of the CB so that the glider motion (saw-tooth or spiral glide) is again enabled. The attitude of the proposed vehicle is sensitive to the mass distribution, hence slight changes of the location of the movable mass or some small leaks of oil may all cause a drastic change of attitude. All these factors need to be discussed carefully to obtain a good attitude control for the proposed vehicle.
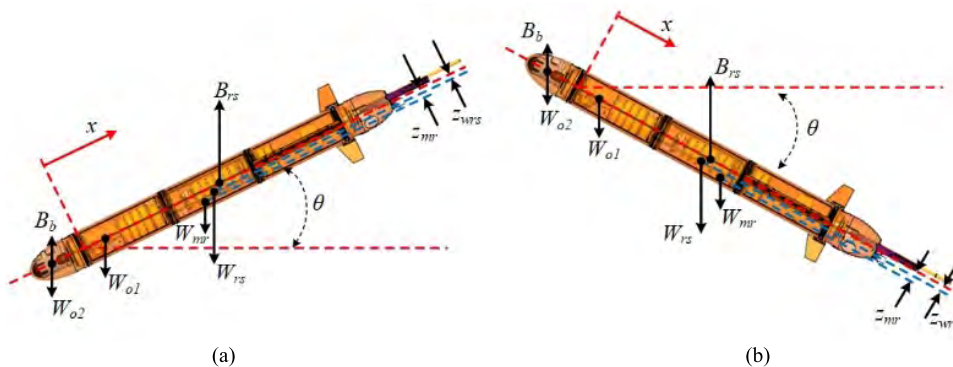
FIGURE 10. Mass distribution of the vehicle in glider mode. To realize the gliding operation for the vehicle, the pitch angle should change repeatedly between a positive value (diving) to a negative one (rising). (a) Mass distribution of diving motion in glider mode. (b) Mass distribution of arising motion in glider mode.

First, consider situations in the Argo mode. To ensure the safe and stable operation of the vehicle in this mode, the relative position of the CG and the CB should be adjusted in a way as shown in Fig. 9 that the CG is under the CB strictly and both of them are on the central axis. To achieve that, the movable mass rotates around the x-axis to the opposite side of the stationary mass with respect to the x-axis, which results in a total CG coinciding with the central axis while the CB remains on the x-axis. Therefore, the equilibrium equations of the vehicle in the steady floating state can be obtained as:

$$\sum F_x : W_{mr} + W_{o1} + W_{o2} + W_{rs} - B_b - B_{rs} = 0 \quad (3)$$

$$\sum M : z_{mr} W_{mr} + z_{wrs} W_{rs} = 0 \quad (4)$$

Then, consider situations in the UG mode. When the movable mass rotates 180° around the centerline with its longitudinal position fixed, the vehicle switches from the profiling float mode to the UG mode. During the transition, the balance of the gravitational moments between the movable mass and the remaining static mass vanishes, and then a following change of attitude such as pitch angle and roll angle occurs. The mass distributions in glider modes during diving and rising are shown in Fig. 10. The vehicle in this mode shares the same equilibrium equations as in (1) and (2).

After vehicle rotates the movable mass to switch to the UG mode, the CGs of m_{mr} and m_{rs} locate on the same side of the x-y plane. In this condition, the vehicle can be operated as a conventional glider. By tuning the movable mass's position, the pitch angle in the neutrally buoyant state can be controlled in a way as the following equation implies (5), as shown at the bottom of this page. For a given oil mass, the parameters B_b, B_{rs}, W_{o1} and W_{o2} in (5) are constant. Then, (5) can be simplified as:

$$\theta = \tan^{-1}(\frac{C - x_{wrs} W_{rs} - x_{mr} W_{mr}}{z_{mr} W_{mr} + z_{wrs} W_{rs}}) \quad (6)$$

$$C = x_b B_b + x_{brs} B_{rs} - x_{o1} W_{o1} - x_{o2} W_{o2} \quad (7)$$

Note that the x_{wrs} is fixed and the x_{mr} is always limited in a predesigned range (x_{mrmin}, x_{mrmax}) for an experimental vehicle. In the UG mode, the CGs of m_{mr} is always limited within a moving range close to the bottom. Therefore, pitch θ is never able to reach $\pm 90°$ no matter how to adjust the buoyancy and attitude systems, which indicates $\theta(-\pi/2, \pi/2)$ when the vehicle glides. In fact, 90° pitch attitude corresponds to the vertical float state in the profiling float mode. Obviously, once the movable mass is set to be free from the rotation limitation and rotates to a certain place that make (4) hold, the vehicle can easily pitch to 90°.

C. OPERATION MODE SWITCH

The innovation of the proposed vehicle is the design combination of the profiling float and the UG so that the proposed vehicle can operate in both the profiling float mode and the glider mode. To have a deep insight into the modal switch mechanism of the proposed vehicle, a cross sectional view in y-z plane as shown in Fig. 11 is considered to illustrate intuitively the internal variation of the vehicle during the modal switch between different operating modes.

For simplified reasoning, the total weight force is denoted as W, i.e. $W = W_{rs} + W_{mr} + W_{o1} + W_{o2}$, and the total buoyancy is denoted as B, i.e., $B = B_{rs} + B_b$. To highlight the variation of the relative position of W and B during the modal transition, the vehicle is assumed neutrally buoyant with $B_{rs} + B_b$-W_{rs}-W_{mr}-W_{o1}-$W_{o2} = 0$. For the proposed vehicle with symmetric shape, the buoyancy acts at the center of the cross section in Fig. 10. Making the vehicle vertically float in Argo mode needs the CG of total weight coinciding with the centerline of the vehicle. Therefore, the movable mass rotates to the place as shown in Fig. 11 (a) where its gravitational moment with respect to the central axis cancels out the one of remain static mass, i.e., (3) holds. Meanwhile, the movable mass is

$$\theta = \tan^{-1}(\frac{x_b B_b + x_{brs} B_{rs} - x_{o1} W_{o1} - x_{o2} W_{o2} - x_{wrs} W_{rs} - x_{mr} W_{mr}}{z_{mr} W_{mr} + z_{wrs} W_{rs}}) \quad (5)$$
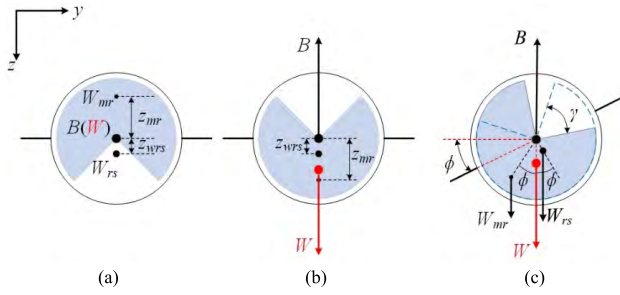
FIGURE 11. Mass distribution of the vehicle in glider mode. To realize the gliding operation for the vehicle, the pitch angle should change repeatedly between a positive value (diving) to a negative one (rising). (a) Argo mode. (b) Initial glider mode. (c) Battery rotates an angle.

FIGURE 12. Frame illustration.

pushed to its forward limiting position so that the CG can be closest to the front of the vehicle and the maximum distance between W and B is reached, which ensures a reliable static stability.

To change from the Argo mode to the UG mode, the vehicle firstly needs to reconfigure the mass distribution to leave the balance in steady vertical float by rotating movable mass 180° around the x-axis. Then the CG of movable mass and remain static mass stay on the same bottom side of the x-y plane as in Fig. 11 (b). Since W is no longer on the x-axis with an offset in the positive z-direction, the vehicle pitches to a non-vertical attitude and is ready for the following glide motion. Fig. 11(c) demonstrates a typical roll maneuver of the proposed vehicle in UG mode by letting the movable mass do a rotation with an angle γ. As seen in the figure, the vehicle consequently obtains a roll angle ϕ in opposite directions. Obviously, for a given γ the roll angle is $\phi = \gamma/2$ when the vehicle loiters at zero velocity in UG mode. The pitch angle θ and yaw angle ψ in this static equilibrium state can be further deduced as follow (8), (9), as shown at the bottom of this page. As stated before, the key to the combination of the concepts of the profiling float and the UG is the novel capability of full rotation for movable mass, i.e., γ [0, 360°]. Theoretically, the vehicle can rotate the movable mass 360° no matter in which mode it is. However, in practice, rotation of the movable mass must be confined within a range when the vehicle is in the UG mode. Because a certain margin of metacentric height needs to be guaranteed so that the vehicle has sufficient static stability to overcome the disturbance like uncertain turbulence and ocean current. The vehicle's metacentric height is equal to distance between the CG and the CB. Only when the CG is below the CB, i.e., the CG locates below the x-y plane, has the vehicle reliable stability. Furthermore, it is the z-coordinate of CG that affects the metacentric height most in UG mode. Therefore, in our simulation and
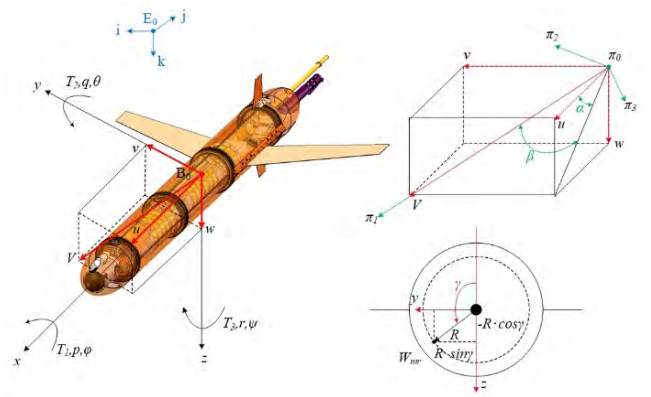
trials, a rotational limitation of the movable mass is set to γ [−90°, 90°] with the definition that $\gamma = 0°$ represents the movable mass is rotated to the most bottom place as depicted in Fig. 11(b) in a glide. As in the rest range of γ, the vehicle is easier to experience a decrease in metacentric height and suffer from some problems such as instable glide, attitude chattering and so on.

III. VEHICLE CHARACTERIZATION RESULTS

The proof-of-concept prototype of the proposed vehicle described in Section II is firstly characterized and is used to verify the attitude regulation principles in Section II. As in Fig. 12, an inertial frame, a body-fixed frame and a current reference frame are used to describe the motion of multimodal underwater vehicles. The inertial frame is represented by an orthonormal axis set $\{\mathbf{i}, \mathbf{j}, \mathbf{k}\}$, where $\mathbf{k}$ is aligned with the local direction of gravity. The body-fixed frame $\boldsymbol{B_0}$-$\boldsymbol{xyz}$ has the origin B_0 coinciding with B_{rs}, the x-axis pointing to the nose, the y-axis pointing to the right, and the z-axis pointing to the bottom. The current reference frame $\{\pi_1, \pi_2, \pi_3\}$ that is used to describe the hydrodynamics forces and moments. The viscous force and moment are most easily expressed in the "current" reference frame [31].

Table 1 gives the specifications of the prototype. Longitudinal translation ranges of movable mass measured from the origin of body-fixed frame is [-0.171m, -0.021m]. As demonstrated in Fig 12, γ is the rotation angle around longitudinal axis $\mathbf{x}$ starting from negative $\mathbf{z}$-axis in a counterclockwise direction, and R is the radial distance of movable mass from the $\mathbf{x}$-axis.

The following operating conditions are evaluated for the prototype: the surface stance, the roll and pitch attitudes during upward and downward gliding, and the attitudes during operation mode switch.

$$\theta = \tan^{-1} \left(\frac{x_b B_b + x_{brs} B_{rs} - x_{o1} W_{o1} - x_{o2} W_{o2} - x_{wrs} W_{rs} - x_{mr} W_{mr}}{z_{mr} W_{mr} \cos \gamma + z_{wrs} W_{rs}} \right) \tag{8}$$

$$\psi = \tan^{-1} \left(\frac{z_{mr} W_{mr} \sin \gamma}{x_b B_b + x_{brs} B_{rs} - W_{o2} x_{o2} - W_{o1} x_{o1} - r_{mrx} W_{mr} - x_{wrs} W_{rs}} \right) \tag{9}$$

TABLE 1. Specifications of the proof-of-concept prototype.

Symbol	Value
Stationary mass m_{rs}	170.6kg
Position of the stationary mass $\mathbf{r}_{rs}$	[0.0125,0,0.0033]m
Inertia of the stationary mass $\mathbf{I}_{rs}$	Diag([3.25, 103.45,104.06])kg·m^2
Movable mass m_{mr}	20kg
Position of the movable mass R	R=0.028m,-π/2$\leq\gamma\leq\pi$,
	-0.021m$\leq r_{mrx}\leq$-0.171m
Net buoyancy m_b	1.5kg$\leq$m$_b\leq$1.5kg
Position of the net buoyancy $\mathbf{r}_b$	[1.52,0,0]m
Displaced fluid mass m	190.6kg
Smartfloat hull diameter D	0.301m
Smartfloat hull length L	3.55m

FIGURE 13. The vehicle in Argo mode.

A. ARGO MODE

It is well known that buoys always remain a vertical upright attitude in the sea. Due to the vertical slender construction and simple inner configuration, it is always convenient and beneficial to arrange the CG and the CB on the central longitudinal axis and make the distance between them long enough to provide the buoy with adequate stability. As for the proof-of-concept prototype changing from UG mode to Argo mode, the movable mass needs to rotate to a certain position so that the CG can converge to the x-axis on which the CB is always fixed. Then the movable mass is driven to the front limiting position to ensure the vehicle with the best stability. The metacentric height of the prototype in Argo mode eventually reach its maximum about 9 mm.

During the float in Argo mode, the prototype maintains a vertical nose-down attitude. In this condition, the vehicle can vertically surface by increasing the displaced volume of the bladder via buoyancy regulation control (shown in Fig. 13). Compared with conventional gliders, the iridium satellite antenna of the proposed vehicle is able to vertically emerge from the surface with 500 millimeter. By doing so, the steady float state on the surface can be preserved over multiple situations, and the communication capabilities of the vehicle including translating the GPS and collecting data and receiving mission instructions are enhanced.
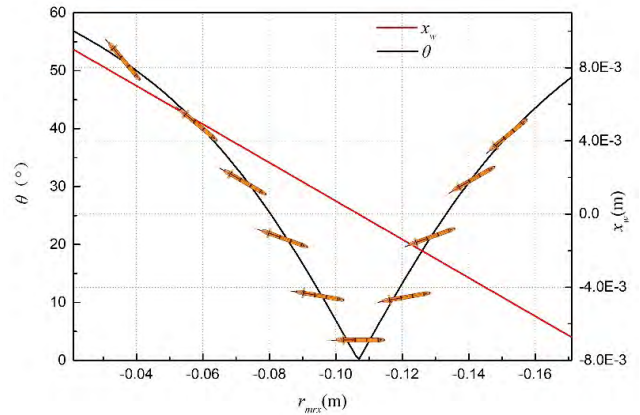
FIGURE 14. The trajectories of x coordinates of the total gravity center (red solid line) and pitch angle of the vehicle (black solid line) change with the translational motion of the movable mass in the x direction from −0.021m to −0.171m. The vehicle is assumed to be neutral buoyant.

B. GLIDER STATE

As stated above, during the glide the CG of movable mass should be kept below the CG of stationary mass for the stable gliding consideration. It is inferred that the best stability is obtained when $\gamma = 0°$. At this point, the distance between the CG and the CB increase to its maximum. In this situation with a given buoyancy, the prototype can obtain various pitch angle by only moving the movable mass longitudinally. Fig. 14 shows the simulation results of this maneuver under the condition that the vehicle is neutral buoyant. From the figure, it can be seen that the **x**-coordinates value of total gravity center, x_w, changes from 0.009 m to −0.00674 m as the movable mass shifts from −0.021 m to -0.171 m. Consequently, the pitch regulation varies from −56.7° (down by head) to +49° (down by stern). Note that y-coordinates value, y_w, and z-coordinates value, z_w, are constant 0 m and 0.0059 m respectively during the pitch regulation. Since y_w is constant zero, roll angle and yaw angle should be absolutely constant zero as well in the absence of disturbance.

In a more physically situation, the movable mass may be require to execute both translational and rotational motions. In this case, all of the three coordinates of the movable mass with respect to the body-fixed frame are likely to change. To simulate this motion, the movable mass was set to translate from -0.021m to −0.171m and rotated from -90° to 90° at the same time. This action is a simple way to evaluate the motion stability of the prototype when it needs to change direction during a glide. When executing the aforementioned maneuver, the gravity center can be calculated by the following equations:

$$x_w = (W_{mr}r_{mrx} + W_{rs}x_{wrs}) / (W_{mr} + W_{rs}) \qquad (10)$$

$$y_w = RW_{mr} \sin\gamma / (W_{mr} + W_{rs}) \qquad (11)$$

$$z_w = (RW_{mr} \cos\gamma + W_{rs}z_{wrs}) / (W_{mr} + W_{rs}) \qquad (12)$$

Fig. 15 shows 3D trajectory of the total gravity center as a result of the compound motion of the movable mass and Fig. 16 presents the attitudes variation contour.
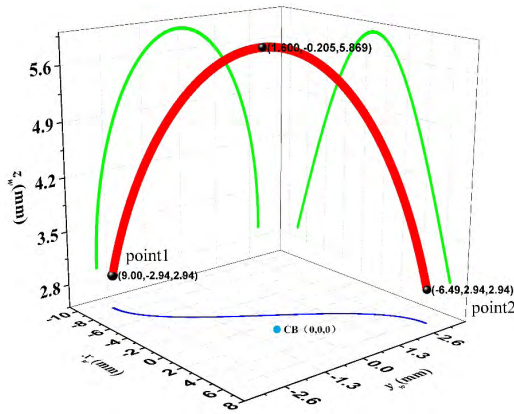
FIGURE 15. 3D trajectory of total gravity center. Green solid line represents the projection of the real gravity center trajectory in XZ plane and YZ plane. Blue solid line represent the projection of the real gravity center trajectory in XY plane. The gravity center moves from point 1 to point 2 while the center of buoyancy is fixed in the origin.

As seen in Fig. 15, the CG was always below the CB with a varying distance over 2.9 mm wherever the movable mass was during the maneuver. This ensured the prototype always had a good static stability when gliding.

As Fig. 16 (a) shows, both of the rotational and translational movement of the movable mass affect the pitch angle. It is obvious that the pitch angle changed dramatically when the movable mass got close to the origin (the CB). The larger the rotate angle γ was, the greater the pitch angle θ would be. Because the denominator of the right-hand side of (7) will decrease as γ increases, and reaches the minimum at the moment when $\gamma = \pm 90°$. As in Fig. 16(a), the vehicle obtained a maximum nose-down pitch at $+72°$ when $r_{mrx} = -0.021$ m and $\gamma = \pm 90°$, and a maximum nose-up pitch at $-66.5°$ when $r_{mrx} = -0.171$ m and $\gamma = \pm 90°$. The influence of the movable mass position on the yaw direction is also illustrated in Fig. 16(b). The translational motion of the movable mass had a significant effect on yaw direction. Notice that a sudden change in the yaw angle happened when the movable mass passed under the CB. When the movable mass was under the CB, the vehicle floated horizontally. In this condition, yaw motion was very sensitive to the movable mass position as (8) implies.
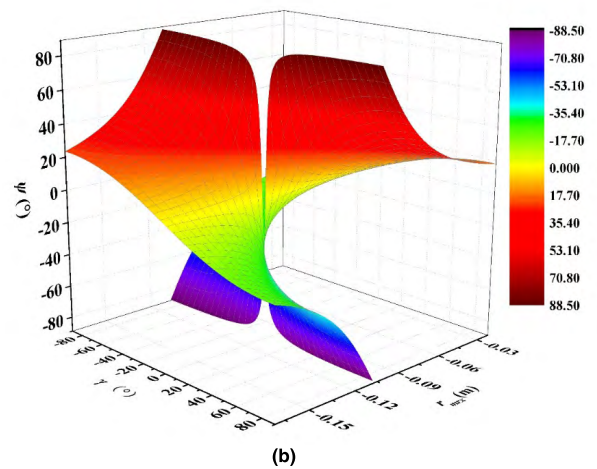
C. MODAL SWITCH

Modal switch is the key transitory stage for the prototype. The success of the transition contributes to the combination of the concepts of conventional glider and buoy without any conflict.

It is noted that the bladder is mounted in the front of the vehicle as shown in Fig. 1, which means that increase or decrease in buoyancy provided by the bladder tend to make the vehicle pitch up. Therefore, to avoid the interference in pitch attitude caused by the buoyancy regulation, with a given buoyancy, the position of the movable mass is the only variable which can influence the CB of the vehicle.
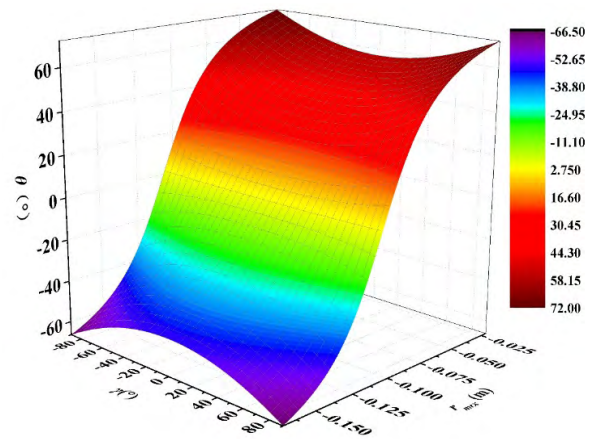
(a)

(b)

FIGURE 16. Variation of pitch angle and yaw angle. The pitch angle achieves its positive maximum at $+72°$ and its negative maximum at $-66.5°$ while the roll angle varies from $+45°$ to $-45°$ in the simulated maneuver.

The modal switch procedure is designed to accomplish step by step including the translational and rotational motions of movable mass. In the designed modal switch scheme for a glider-to-Argo transition, the movable mass is rotated to $\gamma = 0°$ firstly from any possible previous locations. Then the ball-screw-motor system pushes the movable mass to the most front place of its moving range, i.e., $r_{mrx} = -0.021$m. Finally, the movable mass rotates again back to $\gamma = 180°$. After these three steps, the total gravity center coincides with the x-axis, which makes the prototype from horizontal or quasi-horizontal to vertical. Because the movable mass is already in the place closest to the front, the distance between the centers of gravity and buoyancy reaches its maximum. Hence, the prototype obtains the best static stability in Argo mode. When it comes to an Argo-to-glider transition, the only thing needed is repeating the three steps in a reverse order.

The modal switch procedure applied in the prototype was numerically studied. The whole simulation lasted 65 seconds. It was assumed the movable mass started the modal switch process in an initial location with $x_{mr} = -0.1$m and $\gamma = 0°$.
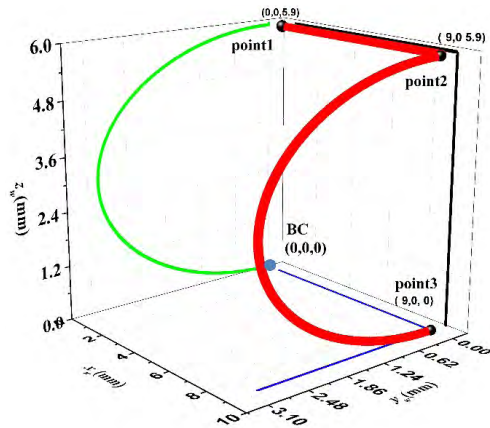
FIGURE 17. 3D trajectory of the centers of the gravity and buoyancy in red. Black solid line represents the projection of the real 3D trajectory onto XZ plane. Green solid line represent the projection of the real 3D trajectory onto YZ plane. Blue solid line represent the projection of the real 3D trajectory onto XY plane. The center of gravity moved from point 1 to point 3 along with the red solid line. The buoyancy center is in (0,0,0).
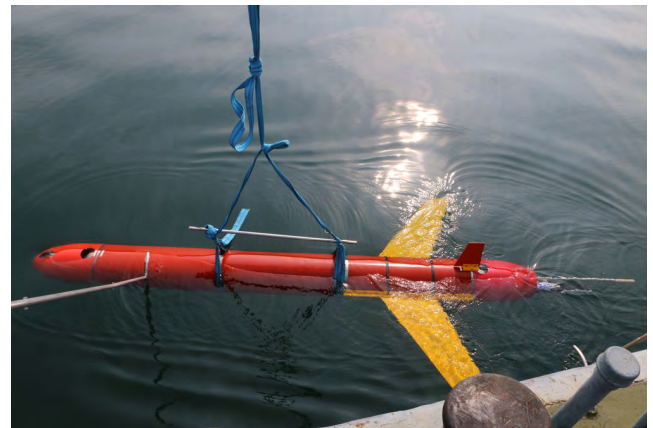

FIGURE 18. variation of pitch angle, roll angle and yaw angle in modal switch simulation.

Movable mass started to move forward at 0s and stopped at 50s. Then it took 10 second to rotate the movable mass from $\gamma = 0°$ to $\gamma = 180°$ followed by loitering at zero velocity for the last 5 seconds. The consequent trajectory of the center of gravity in 3D space is illustrated in Fig. 17. As shown in the figure, the center of gravity moved in the direction parallel to the negative x-axis from point 1 to point 2. Then it continuously moved along a semi-circular path in YZ plane to point 3 which coincided with x-axis.

The attitude responses in the glider-to-Argo transition are demonstrated in Fig.18. Obviously in the first 50 seconds, translational movement of the movable mass made the pitch angle increase from 6.89° to 56.8° while roll and yaw angle remained zero. Then in the next 10 seconds, pitch angle rapidly increased to +90° while roll angle increased from 0° to +90° synchronously as the movable mass rotated from $\gamma = 180°$ to $\gamma = 0°$. However, yaw angle varied in a nonmonotonic changing pattern. From 50 s to 55 s, yaw angle tended to rise. After reaching the maximum value of about

FIGURE 19. The test in Fu Xian Hu Lake.

18° at 55 s, yaw angle started to decreased and became zero again at 60 s. Although the roll and yaw angles changed with the modal switch process, the values of the two angles were insignificant to the prototype when it floated vertically in Argo mode. It should be noticed that the prototype is subject to the gimbal lock problem when floating vertically. Because there is no such a rotation around the **z** axis that can make the vehicle back to its former orientation after the vehicle rotates around the **x** axis. It means that the Eulerian method to describe the yaw direction is not suitable in this situation at all. Therefore, the vertical operating condition should be dealt with carefully for designing effective control strategies for the proposed vehicle.
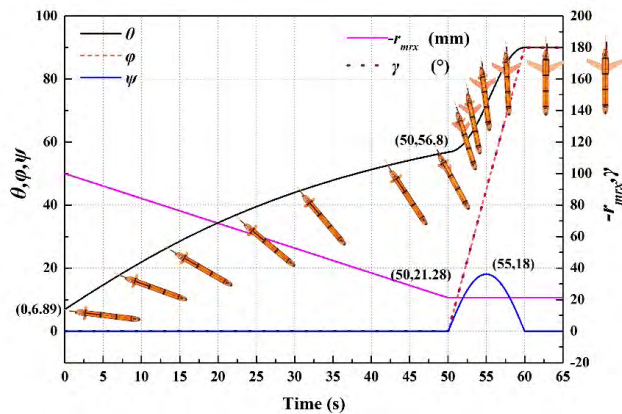
IV. EXPERIMENTS OF THE MULTI-MODE UNDERWATER VEHICLE
The most significant performance of the vehicle is motion switch, navigation-keeping and sawtooth glide performance. In this section, experiments in field trials are introduced to investigate the performance and maneuverability of the multimodal underwater vehicle. The tests were performed in Fu Xian Lake in Yun Nan province.

A. THE MODE SWITCH EXPERIMENTS
Mode switch ability is the most prominent feature of the *Smartfloat*. By enabling both of the Argo and glider operation modes, the *Smartfloat* possesses the capabilities that those previous single-modal platforms have, and therefore makes itself competent in more complex mission scenarios. An experiment was carried out to demonstrate the switch ability of the *Smartfloat* from the glider mode to the Argo mode, and the results are exhibited in Fig. 20.

In the experiment, the vehicle was initially floated at the surface with a pitch angle of $-20°$ by setting $\gamma = 0°$ and $r_{mrx} = -0.116$ m. The switch action composed of two steps. The first step was shifting the movable mass along with the x-axis to the place at $r_{mrx} = -0.021$. From Fig. 20, it can be observed that the pitch angle reached to $-70°$ after the translational motion of the movable mass finished at 90 s. Then the second step (from 93 s to 102 s) was rotating the movable
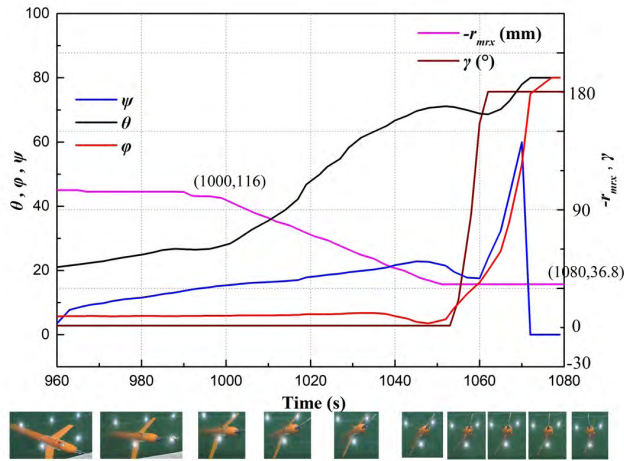
FIGURE 20. Variation of pitch angle, roll angle and yaw angle in mode switch test.

mass by 180° so that the CG could eventually coincided with the **x**-axis. The pitch angle had kept increasing from −70° since the movable mass started to rotate, and it finally maintained at −90°. Meanwhile, the roll angle increased fast to 90°. It should be emphasized that the pitch and roll response recorded in Fig. 20 has a maximum value of 80° instead of 90° due to the limitation of the attitude sensor's range from −80° to 80°. Moreover, when the vehicle successfully switched to the Argo mode and floated vertically, it was subjected to the gimbal lock problem. Therefore, a sudden change in the yaw direction happened and the yaw angle data was meaningless.

B. THE SAWTOOTH GLIDE EXPERIMENTS

The data from saw-tooth tests are given in Fig. 21. The target depth of the vehicle during the sawtooth was set as 70m. Because the flow limitation of the buoyancy control system, the target depth was overshot by about 5m. The descent and ascent pitch angle were set as ±25°.

At the beginning of a mission profile, the vehicle floated at the surface in Argo mode with a head down attitude so that the Iridium satellite antenna could emerge from water and acquired a good communication condition. After finishing the instruction transmission, the vehicle switched to the glider mode in a short time, and then descended by reducing buoyancy and changing the attitude. In Fig. 21(a), notice that the pitch angle had a drastic variation from 0 s to 625 s. This is because the movable mass was rotated simultaneously during the buoyancy regulation to make the vehicle enter the glider mode and get the vehicle ready for the following gliding motion. In addition, it should be pointed out the external bladder was mounted in the head so the buoyancy regulation would affect the pitch attitude to some extent. When descending, the oil was pumped into the inner tank from the outside bladder. As the displaced volume of the bladder decreased, the restoring moment generating by the buoyancy and the gravity changed and consequently resulted in a variation of pitch angle.
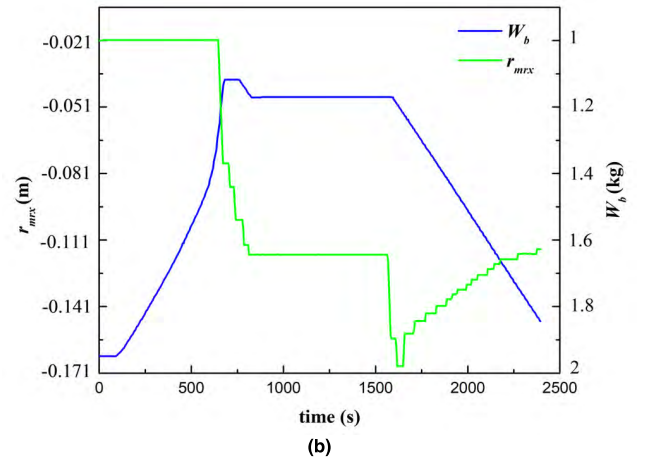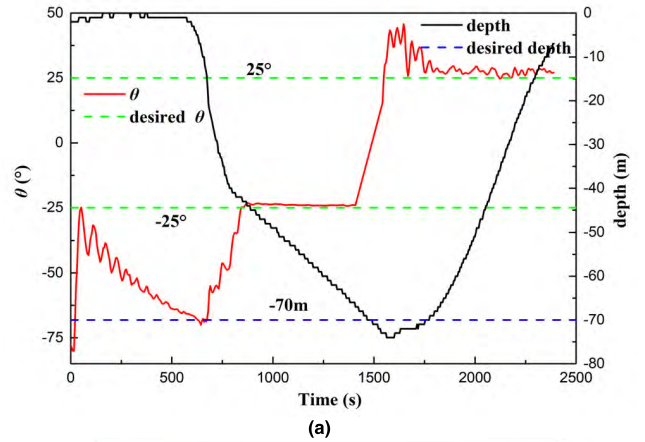

(a)

(b)

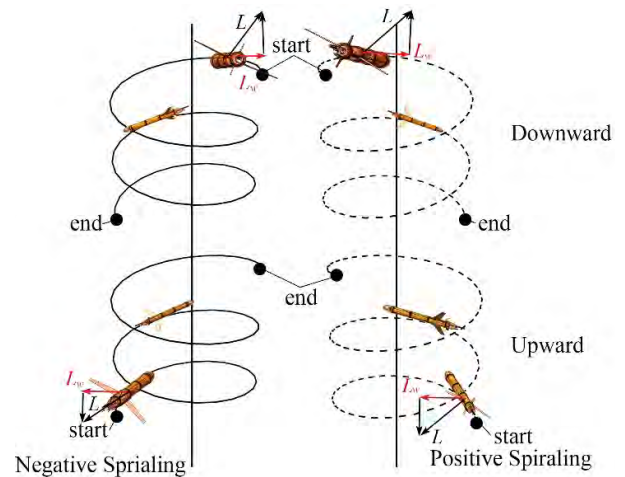**FIGURE 21.** Sawtooth glide test result.

FIGURE 22. The relationship between the vehicle system and spiral trajectory.

In the field trials, it was hard for the vehicle to maintain stable under the wave disturbance when the vehicle floated at the surface. So an obvious oscillation of pitch angle can be observed in Fig. 21(a). But the results also demonstrate the good tracking performance of the attitude control system with fast tracking speed and stability in both of the descent and ascent stage.
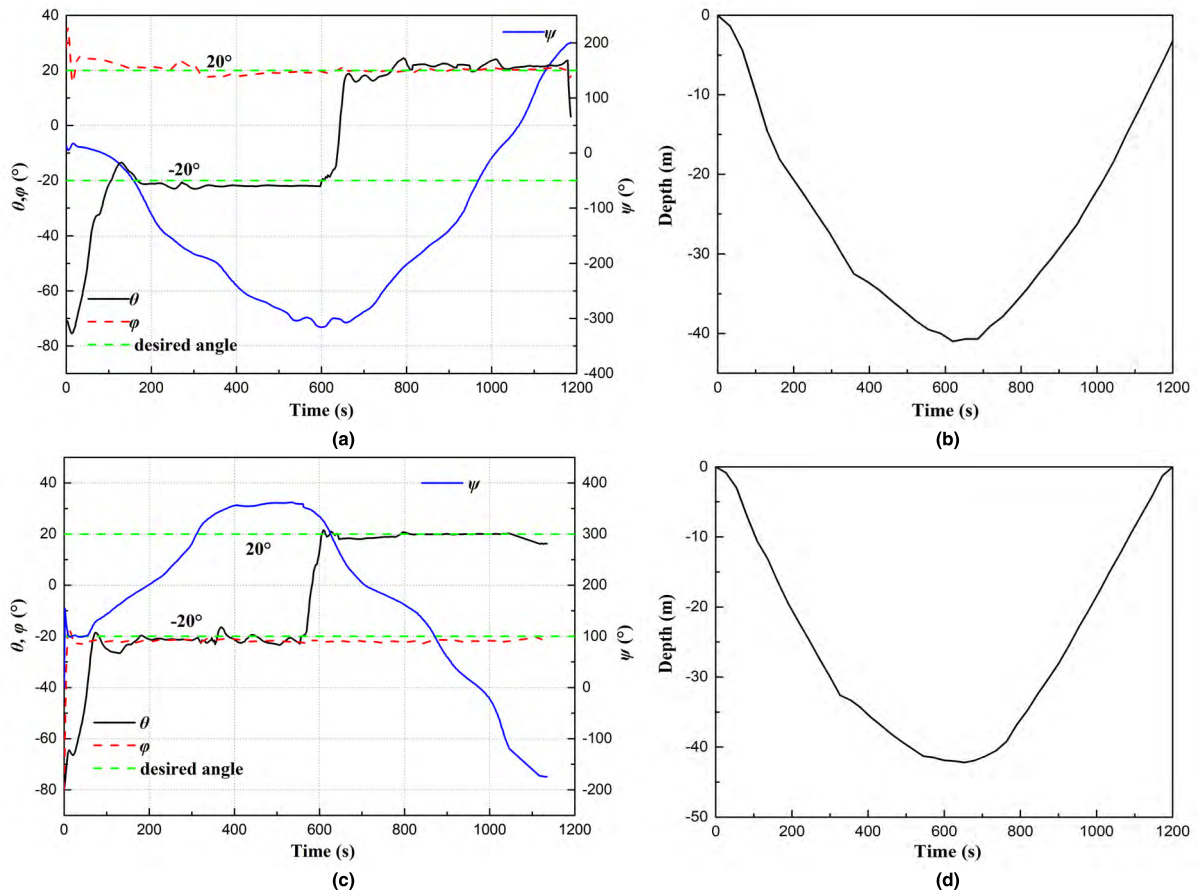
FIGURE 23. The spiral glide test results. (a) and (b) record the attitude and depth responses of the vehicle in the first test; (c) and (d) record the attitude and depth responses of the vehicle in the second test.

C. THE TURNING GLIDE EXPERIMENTS

The turning glide experiments were used to verify the spiral motion pattern and analyze the course-keeping performance of the *Smartfloat*. To know the spiral pattern of the vehicle, experiments were conducted by making the vehicle keep some certain roll angles and pitch angles during the ascent and descent stages in order to evaluate the performance and stability of turning process.

Unlike a conventional aircraft, the underwater gliders exhibit different roll/yaw relationships in the downwards glide and upwards glide respectively, which leads to different spiral motion. For the sake of simplifying the discussion, this paper defines the positive and negative spiraling motion as shown in Fig. 22. The positive spiral is defined as the spiraling motion in which the horizontal component of the lift force, L_w, points to the axis of the spiraling trajectory. The negative spiral is defined as the spiraling motion in which the L_w points away from the axis of the spiraling trajectory. The kind of spiraling motion a glider can execute is determined by the vehicle's hydrodynamics that is related to the airfoil profile, the outline of the body, and the wing's position. Among all these factors, the wing's position has the most significant influence on the direction of the spiraling motion.

Differing from most underwater gliders, the *Smartfloat* had a pair of aft-mounted wings. So it could be inferred that the *Smartfloat* would perform a negative spiraling. That means a roll to the right (left) would make the lift force point away from the axis of the spiral path and consequently resulted in a yaw to the left (right) in the descent. Similarly, a roll to the right (left) would generate the lift force pointing away from the axis of the path and therefore produce a yaw to the right (left) in the ascent.

The results of the spiraling motion tests are shown in Fig. 23. In the experiments, two groups of turning test, each of which includes a downwards glide to 40 m depth with a pitch angle of $-20°$ and an upwards glide with a pitch angle of $20°$, were conducted. Note that every experiment was started with the vehicle in the Argo mode floating at the surface. Therefore, the vehicle changed to the glider mode at first and then executed the spiraling motion.

The first test requires a roll to the right with $20°$ while the second test requires a roll to the left with the same angle. In Fig. 23, the yaw turned to the left (right) when the vehicle glided downwards (upwards) with a roll to the right, and turned to the right (left) when the vehicle glided downwards (upwards) with a roll to the left. Therefore, the results
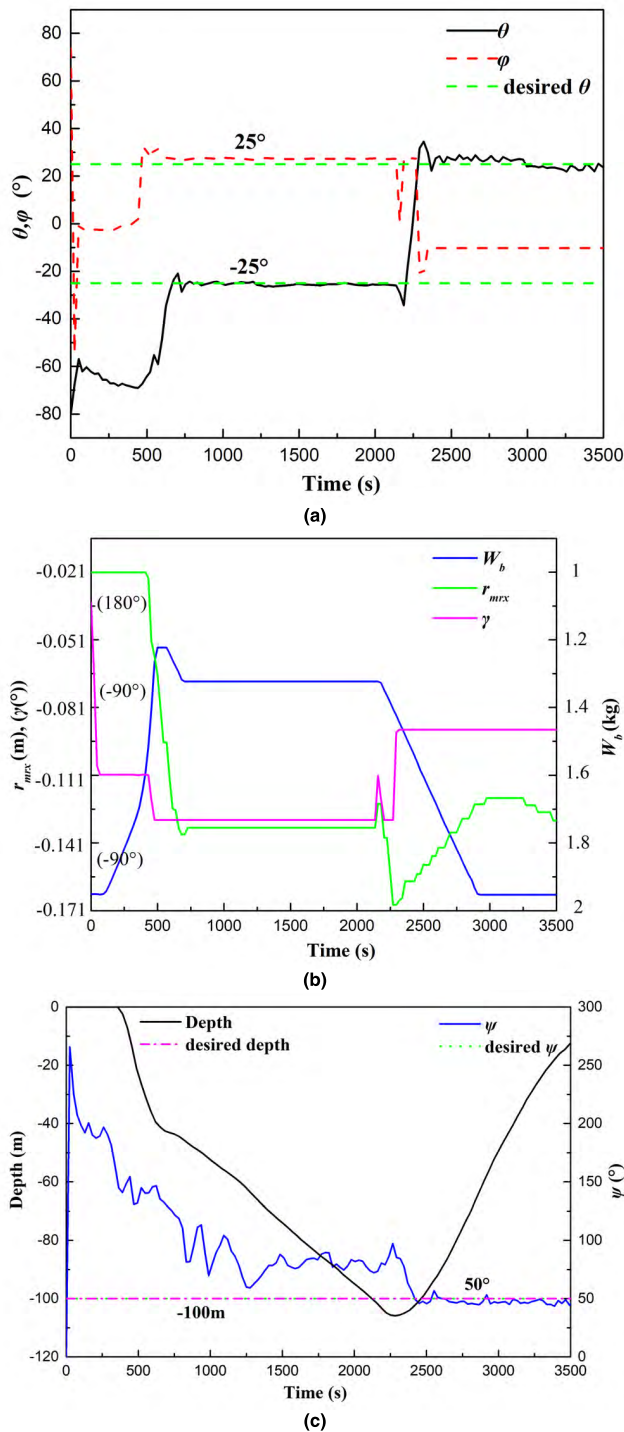
FIGURE 24. The navigation-keeping glide test results. (a) The roll and pitch angle responses; (b) behaviors of actuators (the movable mass and the external bladder); (c) the depth and yaw angle responses.

verify that the *Smartfloat* was doing a negative spiraling motion when it turned.

Another groups of tests were then carried out to evaluate the course-keeping performance of the vehicle. In these tests, the pitch angles in the ascent and descent were set as $\pm 25°$ respectively. Target depth was 100 m and the target

yaw direction was 50°. The results are exhibited in Fig. 24. From Fig. 24 (a) and (b), it can be seen that the pitch angle could converge to the target value well and the actuators (the movable mass and the buoyancy control system) did not encounter with the chattering problem. All the control process was smooth and stable. The yaw response recorded in Fig. 24(c) proves that the vehicle successfully fulfilled the yaw tracking mission by executing the negative spiraling glide and had the good ability of course-keeping. However, due to the hysteretic characteristic of the buoyancy control system, the depth control response had an overshoot of about 9 m.

V. CONCLUSION

A novel platform that combines both of the Argo mode and the glider mode is proposed in this paper, and it is successfully realized by a novel attitude control system. The attitude control system enables a rotation of 360° of the movable mass (a movable battery pack with an eccentric mass distribution) around the x-axis. Therefore, the CG can not only move in the manner as a conventional underwater glider does but also shift in the longitudinal axis where the CB locates, which is the key of combining the mobility of the profiling float and the glider for a single platform.

A prototype, called the *Smartfloat*, was fabricated with the utilization of the proposed attitude control system. The preliminary motion principles of the prototype in different modes were deduced under the conditions that the vehicle was neutral buoyant. Then, the prototype was characterized and its attitude regulation performance was tested numerically in different operation modes. Finally, the field trials were carried out to test the functions of the prototype. In the experiments, the vehicle successfully executed the modal switch, the vertical diving and surfacing and depth keeping in the Argo mode, and the sawtooth glide and the spiral glide in the glider mode. The results verify the feasibility of the proposed multi-modal platform and demonstrate the vehicle's good performance in different operation modes.

REFERENCES

[1] D. P. Chambers, A. Cazenave, N. Champollion, H. Dieng, W. Llovel, R. Forsberg, K. von Schuckmann, and Y. Wada, ''Evaluation of the global mean sea level budget between 1993 and 2014,'' *Surv. Geophys.*, vol. 38, no. 1, pp. 309–327, 2016.

[2] W. Llovel, S. Guinehut, and A. Cazenave, ''Regional and interannual variability in sea level over 2002–2009 based on satellite altimetry, Argo float data and GRACE ocean mass,'' *Ocean Dyn.*, vol. 60, no. 5, pp. 1193–1204, 2010.

[3] R. Lumpkin and M. Pazos, ''Measuring surface currents with Surface Velocity Program drifters: The instrument, its data, and some recent results,'' in *Lagrangian Analysis and Prediction of Coastal and Ocean Dynamics*. 2007, pp. 1–47.

[4] L. Jian, C. Rongyu, and W. Sheng'an, "Development of international marine observation system and construction of deep-sea station in China," *J. Tropical Oceanogr.*, vol. 31, no. 2, pp. 123–133, 2012.

[5] R. Srinivasan, S. Zacharia, T. Sudhakar, and M. A. Atmanand, "Indigenous drifting buoys for the Indian Ocean observations," in *Proc. OCEANS*, vol. 145, Sep. 2016, pp. 1–6.

[6] L. Barker, "Closed-loop buoyancy control for a coastal profiling float," MBARI, Moss Landing, CA, USA, Intern Rep. 2014-08, 2014, pp. 1–15.

[7] *US Argo Data Assembly Center Documentation Processing System*, Oper. Syst. Sites, Property Initiatives Underwriting Agency Document., Petersfield, U.K., 2011.

[8] Z. Liu, "Fifteen years of ocean observations with China Argo," *Adv. Earth Sci.*, vol. 31, no. 5, pp. 445–460, 2016.

[9] L. Braby, B. C. Backeberg, I. Ansorge, M. J. Roberts, M. Krug, and C. J. C. Reason, "Observed eddy dissipation in the Agulhas current," *Geophys. Res. Lett.*, vol. 43, no. 15, pp. 8143–8150, 2016.

[10] D. L. Rudnick, "Ocean research enabled by underwater gliders," *Annu. Rev. Mar. Sci.*, vol. 8, no. 1, pp. 519–541, 2016.

[11] F. Zhang, "Cyber-maritime cycle: Autonomy of marine robots for ocean sensing," *Found. Trends Robot.*, vol. 5, no. 1, pp. 1–115, 2016.

[12] J. Yu, F. Zhang, A. Zhang, W. Jin, and Y. Tian, "Motion parameter optimization and sensor scheduling for the sea-wing underwater glider," *IEEE J. Ocean. Eng.*, vol. 38, no. 2, pp. 243–254, Apr. 2013.

[13] E. E. Heslop, S. Ruiz, J. Allen, J. L. López-Jurado, L. Renault, and J. Tintoré, "Autonomous underwater gliders monitoring variability at 'choke points' in our ocean system: A case study in the Western Mediterranean Sea," *Geophys. Res. Lett.*, vol. 39, no. 20, pp. 1–6, Oct. 2012.

[14] F. Zhang, "Modeling, design and control of gliding robotic fish," Dept. Elect. Eng., Michigan State Univ., East Lansing, MI, USA, Tech. Rep. 3634937, 2014, pp. 10–45.

[15] B. L.-K. Reed, "Controller design for underwater vehicle systems with communication constraints," Ph.D. dissertation, Massachusetts Inst. Technol., Cambridge, MA, USA, 2015.

[16] J. Sherman, R. E. Davis, W. B. Owens, and J. Valdes, "The autonomous underwater glider 'Spray'," *IEEE J. Ocean. Eng.*, vol. 26, no. 4, pp. 437–446, Oct. 2001.

[17] D. C. Webb, P. J. Simonetti, and C. P. Jones, "SLOCUM: An underwater glider propelled by environmental energy," *IEEE J. Ocean. Eng.*, vol. 26, no. 4, pp. 447–452, Oct. 2001.

[18] C. C. Eriksen, T. J. Osse, R. D. Light, T. Wen, T. W. Lehman, P. L. Sabin, J. W. Ballard, and A. M. Chiodi, " Seaglider: A long-range autonomous underwater vehicle for oceanographic research," *IEEE J. Ocean. Eng.*, vol. 26, no. 4, pp. 424–436, Oct. 2001.

[19] A. Wolek, E. M. Cliff, and C. A. Woolsey, "Time-optimal path planning for a kinematic car with variable speed," *J. Guid., Control, Dyn.*, vol. 39, no. 10, pp. 2374–2390, 2016.

[20] A. Wolek and C. Woolsey, "Feasible Dubins paths in presence of unknown, unsteady velocity disturbances," *J. Guid., Control, Dyn.*, vol. 38, no. 4, pp. 782–787, 2015.

[21] A. Wolek, T. Gode, C. A. Woolsey, J. Quenzer, and K. A. Morgansen, "Testing a pneumatic underwater glider in shallow water," in *Proc. IEEE/MTS OCEANS*, Oct. 2015, pp. 1–8.

[22] C. Woolsey, "Vehicle dynamics in currents," Virginia Center Auton. Syst., Tech. Rep. VaCAS-2011-01, 2011, pp. 1–29.

[23] P. G. Thomasson and C. A. Woolsey, "Vehicle motion in currents," *IEEE J. Ocean. Eng.*, vol. 38, no. 2, pp. 226–242, Apr. 2013.

[24] S. Fan and C. A. Woolsey, "Dynamics of underwater gliders in currents," *Ocean Eng.*, vol. 84, pp. 249–258, Jul. 2014.

[25] M. Y. Javaid, M. Ovinis, T. Nagarajan, and F. B. M. Hashim, "Underwater gliders: A review," in *Proc. MATEC Web Conf.*, vol. 13, pp. 02020-1–02020-5, Jul. 2014.

[26] C. Waldmann, A. Kausche, M. Iversen, A. Pototzky, G. Looye, S. Montenegro, R. Bachmayer, and D. Wilde, "MOTH-An underwater glider design study carried out as part of the HGF alliance ROBEX," in *Proc. IEEE/OES Auton. Underwater Vehicles (AUV)*, Oct. 2014, pp. 1–3.

[27] A. Alvarez, B. Garau, and A. Caiti, "Combining networks of drifting profiling floats and gliders for adaptive sampling of the Ocean," in *Proc. IEEE Int. Conf. Robot. Automat.*, Apr. 2007, pp. 157–162.

[28] J. Cao, D. Li, Z. Zeng, B. Yao, and L. Lian, "Drifting and gliding: Design of a multimodal underwater vehicle," in *Proc. MTS/IEEE Kobe Techno-Oceans (OTO)*, May 2018, pp. 1–7.

[29] J. G. Graver, "Underwater gliders: Dynamics, control and design," Ph.D. dissertation, Princeton Univ., Princeton, NJ, USA, 2005.

[30] R. N. Smith and V. T. Huynh, "Controlling buoyancy-driven profiling floats for applications in ocean observation," *IEEE J. Ocean. Eng.*, vol. 39, no. 3, pp. 571–586, Jul. 2014.

[31] J. Cao, J. Cao, B. Yao, and L. Lian, "Three dimensional model, hydrodynamics analysis and motion simulation of an underwater glider," in *Proc. OCEANS*, 2001, pp. 1–8.
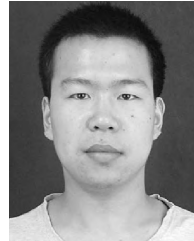
JUNJUN CAO (S'16) was born in China, in 1989. He received the B.S. degree in ship and ocean engineering from Harbin Engineering University, in 2011. He is currently pursuing the Ph.D. degree with the State Key Laboratory of Ocean Engineering, Shanghai Jiao Tong University (SJTU).

His research interests include underwater vehicles, nonlinear time-varying systems, adaptive control, and path planning of underwater vehicles.

DI LU received the B.Eng. degree in naval architecture and ocean engineering from the Huazhong University of Science and Technology, Wuhan, China, in 2015. He is currently pursuing the Ph.D. degree in naval architecture, ocean and civil engineering with Shanghai Jiao Tong University, Shanghai, China.

His research interests include underwater vehicles, hybrid aerial underwater vehicles, nonlinear time-varying systems, adaptive control, and backstepping control.

DAIWEI LI (S'16) was born in China, in 1993. He received the B.S. degree in mechanical engineering from the China University of Petroleum-Beijing (CUPB), in 2016. He is currently pursuing the Ph.D. degree with the State Key Laboratory of Ocean Engineering, Shanghai Jiao Tong University (SJTU).

His research interests include dynamics and automatic control of underwater vehicles.
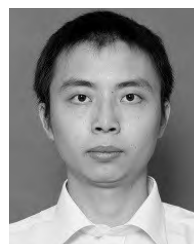
ZHENG ZENG received the B.Eng. degree in electrical and electronic engineering from Hunan University, Changsha, China, in 2010, and the Ph.D. degree from Flinders University, Adelaide, SA, Australia, in 2015.

He is currently an Assistant Research Professor with Shanghai Jiao Tong University, Shanghai, China. He is the Project Leader for multiple projects funded by Shanghai Sailing Program, Qingdao National Laboratory for Marine Science and Technology, and National Natural Science Foundation of China. His research interests include autonomous marine vehicles, including optimal guidance, navigation, and control systems.

BAOHENG YAO received the B.S. degree in mechanical engineering from Fuxin Mining Institute, in 1994, and the Ph.D. degree in mechatronics engineering from Shanghai Jiao Tong University, in 2005. He is an Associate Professor with Shanghai Jiao Tong University, China. His research interests include nonlinear dynamics, fluid mechanics, and subsea technology.

LIAN LIAN received the B.S. and M.S. degrees in naval architecture and ocean engineering and the Ph.D. degree in technology management from Shanghai Jiao Tong University, Shanghai, China, in 1982, 1985, and 2012, respectively.

She has been a Full Professor with Shanghai Jiao Tong University since 1998, and served as a member of Expert Group of National Hi-Tech Program (863 Program) from 1999 to 2011, and a member of Expert Group of the National Science Foundation of China from 2008 to 2011. She is currently the Vice Dean of the Institute of Oceanography, Shanghai Jiao Tong University, and a member of the IEEE/OES Administrative Committee, as well as the IEEE/OES Shanghai Chapter Chair. Her research mainly focuses on underwater vehicles and marine observation. She has been in charge of eight projects as PI/Chief Designer with total funding over 90 million RMB, which include national and municipal research projects funded by the National Hi-Tech 863 Program, National Key Project, National Natural Science Foundation of China, National R&D Program of Marine Technology, as well as the R&D Program of Science and Technology Committee of Shanghai Municipal Government.

• • •